ARIES-ACT1 POWER CORE ENGINEERING

M. S. Tillack[1], X. R. Wang[1], S. Malang[2], F. Najmabadi[1] and the ARIES Team

[1]*UC San Diego, 9500 Gilman Drive, La Jolla, CA 92093-0417, mtillack@ucsd.edu*
[2]*Fusion Nuclear Technology Consulting, Linkenheim, Germany, smalang@web.de*

ARIES-ACT1 is an advanced tokamak power plant conceptual design that utilizes SiC composite structural material in the blanket and PbLi as the tritium breeder and coolant. This design concept represents an evolutionary step from ARIES-AT, which has guided tokamak research programs for the past decade. In conjunction with a helium Brayton power cycle, the high primary coolant outlet temperature allows thermal conversion efficiency of 58%. The self-cooled blanket and He-cooled W-alloy divertor provide the ability to survive relatively high power density with acceptable projected lifetime. In ARIES-ACT1, we attempted to add "robustness" to the design point without major sacrifices in performance. In this paper, we will discuss the main features of the power core and selected details in the design and analysis.

I. INTRODUCTION

The design space for tokamak power plants depends very much on current assumptions on both progress in plasma confinement and technology advances. In order to "chart out" this space, we are examining the "four corners" of design space that is bracketed by relatively more conservative and relatively more aggressive cases.[1] ACT1 is the first detailed design study to be completed, using aggressive plasma parameters (such as β_N=5.75) and aggressive technology choices (such as SiC composite structures operating in the range of 1000˚ C). This corner of design space resembles ARIES-AT.[2]

Since the ARIES-AT study was completed, research results have added constraints on both the plasma and the surrounding structures. For example, the expected peak heat flux in the divertor has increased as a result of new scaling laws for the power decay length in the scrape-off layer, and the presence of transient events like ELMs appears likely. In addition to new external constraints, we have taken this opportunity to perform more detailed design and analysis on several in-vessel components, which has led to new design innovations and more detailed analysis.

In this paper, several new power core features and analyses will be highlighted, including:
(1) a He-cooled steel structural ring around the blanket,
(2) a He-cooled tungsten-alloy divertor,
(3) revised flow paths and manifolding for PbLi to reduce 3D MHD effects,
(4) detailed thermal and stress analysis of the blanket,
(5) integration of multiple coolant streams into a self-consistent power cycle.

Table I summarizes the main device parameters for ARIES-ACT1. The design was selected by scanning a large set of possible plasma equilibria, building and costing a power plant around those plasmas, and then screening the solutions to meet certain performance metrics including low cost of electricity.

Surface heat fluxes in the table are time-averaged. Instantaneous heat fluxes will be higher as a result of transients such as ELMs. *Note, this set of design parameters was generated after substantial analysis of individual components, some of which may have used an earlier set of reference parameters. As the design is still evolving, these may not be the final parameters for the ACT1 design.*

TABLE I. ARIES ACT1 Major Device Parameters

Parameter		**Value**	**Units**
Major radius	R	6.25	m
Aspect ratio	A	4	
Elongation	κ	2.1	
Toroidal field on axis	B_o	6	T
Normalized plasma beta	β_N	5.75	
Plasma Current	I_p	10.9	MA
Fusion power	P_f	1813	MW
Thermal power	P_{th}	2016	MW
Recirculating power		154	MW
Net electric power	P_e	1000	MW
Avg. neutron wall load at FW	P_n	2.3	MW/m^2
Max. neutron wall load at FW		3.6	MW/m^2
Thermal conversion efficiency	η_{th}	57.9	%

II. POWER CORE CONFIGURATION AND MAINTENANCE CONCEPT

Figure 1 shows a cross section of the power core, which is described in further detail elsewhere.[3] The plasma is surrounded by breeding blankets and divertor target plates, which are combined with a steel structural ring to form the life-limited replacement units. Each sector contains a single replacement unit that is maintained horizontally through large ports between TF coils. In this design, the vacuum vessel is located behind the replacement units, with additional permanent magnet shielding located *outside* the vessel.

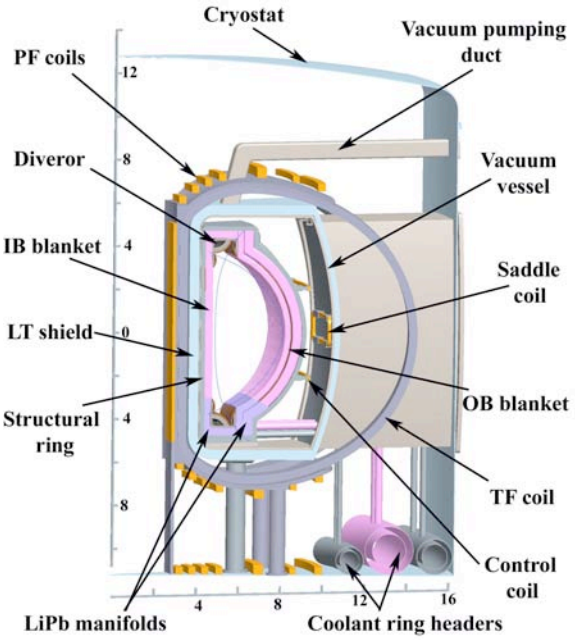

Fig. 1. Cross section of ARIES-ACT1 power core

Power core gravity loads are transferred to the main support pillars through the floor of the vacuum vessel (see Figure 1). All in-vessel components (blankets, divertors, rf systems and coolant manifolding) are attached to a stiff, poloidally-continuous "structural ring" made of high-temperature steel and cooled by He. The use of a steel structural ring is a departure from the ARIES-AT design, which used only PbLi-cooled SiC components inside the vacuum vessel. Besides supporting the in-vessel components and providing mechanical strength to the sectors, the steel ring helps to shield the permanent components and captures a significant amount of energy at high temperature for power conversion. Figure 2 is an expanded view of a replacement unit.

The vacuum vessel, which surrounds the power core, is designed as a container for the high vacuum, the tritium inventory and all radioactive products in the vessel generated by the irradiation. It also serves as a first barrier in case of pressurization by in-vessel coolant leaks or pipe ruptures. The vacuum vessel is not used to support gravity loads of any other component. A 3Cr-3WV bainitic steel alloy was chosen to eliminate the need for post-weld heat treatment of the vessel and to avoid the relatively high activation of austenitic steels.[4]

Between each pair of TF coils, large horizontal ports are arranged at the torus mid-plane, allowing the insertion or extraction of entire sectors in the horizontal direction using a rail system[3]. For the replacement of blankets, divertor targets or other in-vessel components, the outer flange of the maintenance port of a sector is opened and all of the coolant access pipes to the sector are cut. After this operation, the sector is removed horizontally into a maintenance flask, and is replaced in reverse order by a refurbished unit contained already in the flask. The doors of the flask and port are then closed and the flask is transported to a hot cell. Inside the hot cells, components to be replaced are separated from the structural ring and replaced by new ones. Refurbished sectors are moved to the maintenance ports for future use.

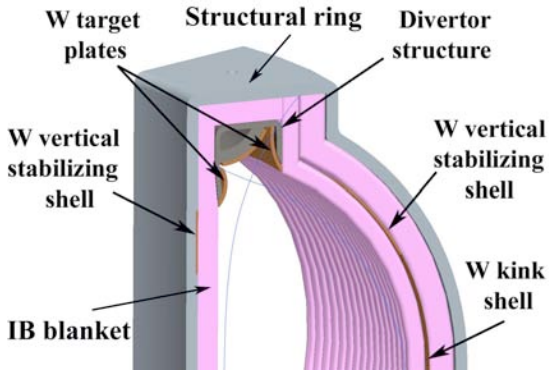

Fig. 2. Details of the replacement unit upper half

III. DIVERTOR

The divertor is used to control plasma exhaust. Its target plates experience the highest surface heat flux of any component in a tokamak. Since such a large fraction of the total fusion power impinges on the divertor, the recovery of heat at high temperature is important for efficient electricity generation. At 10.6 MW/m^2 peak time-averaged local heat flux (see Table II), SiC plasma-facing structures cannot be maintained within their temperature and stress limits. We chose to adopt tungsten alloy structures with He coolant, similar to the ARIES-ST study[5]. This material choice has received considerable design effort[6] and is the subject of ongoing R&D efforts.[7] The use of He in impinging jet configurations has been explored extensively in this project and elsewhere,[8] and has been shown capable of removing heat fluxes in this range, up to ~14 MW/m^2.

TABLE II. ARIES ACT1 Divertor Parameters

Parameter	Value	Units
Coolant	He	
Coolant pressure	10	MPa
Surface power to divertor	276	MW
Peak time-averaged heat flux	10.6	MW/m^2
Peak heat flux during ELMs	4.25	GW/m^2
Inboard slot length	48	cm
Outboard slot length	76	cm
Armor thickness	5	mm
W-alloy structure min allowable T	800	C
W-alloy structure max allowable T	1300	C
W armor max allowable temp	2190	C
He inlet temperature	700	C
He outlet temperature	800	C

The divertor consists of three target plates (inner, outer and dome) plus the mechanical support structures and manifolding. The strike points for the edge plasma occur on the inner and outer plates, close to the pumping ducts. Plasma exhaust is evacuated behind the dome, which allows adequate space for conductance to the inner and outer slots. Figure 2 shows the layout of these elements. In order to provide adequate slot length for the divertor plasma solution on the inboard side we reduced the inboard blanket thickness behind the divertor, which is possible due to the lower neutron flux at this location.

Four design variations were explored in depth for the ARIES-ACT divertor target plates: plate-type, T-tube, finger and integrated plate/finger. All of these are discussed in more detail elsewhere.[6] The main distinction is the use of either linear "slot" jets or an array of circular jets, and the means of feeding and manifolding the He coolant. For the finger and T-tube designs, pure (non-structural) W armor is castellated and brazed onto the W-alloy substrate in order to provide additional resistance to plasma erosion and transients. For the plate-type divertor, the front plate itself is castellated to create an armor zone. We assume the armor can operate up to 2/3 the melting point of W, because it does not carry loads. In all cases, a transition joint is located outside the high heat flux region, where the W-alloy heat sink is bonded to steel coolant supply lines through an intermediate Ta layer to accommodate differential stress.[9]

Figure 3 shows the results of detailed 3D thermal analysis using ANSYS multi-physics software.[10] Here we have plotted the coolant pumping power required to maintain all structures within their operating temperature limits (see Table II) as a percentage of the incident thermal power. While there is no absolute limit, designs with more than 10-15% pumping power are avoided. Note: all of the pumping power is recovered as high-grade heat, which is then converted to electricity at the plant power conversion efficiency (which is >50%). This reduces the effect on plant net efficiency, but increases recirculating power and the size of heat transfer and power conversion equipment.

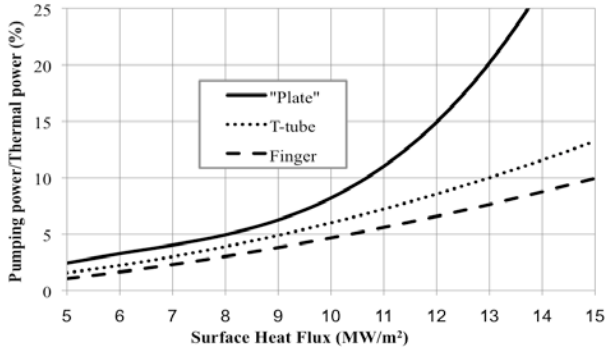

Fig. 3. Comparison of pumping power for the three main divertor concepts (these results were obtained using 600/700 C inlet/outlet temperature).

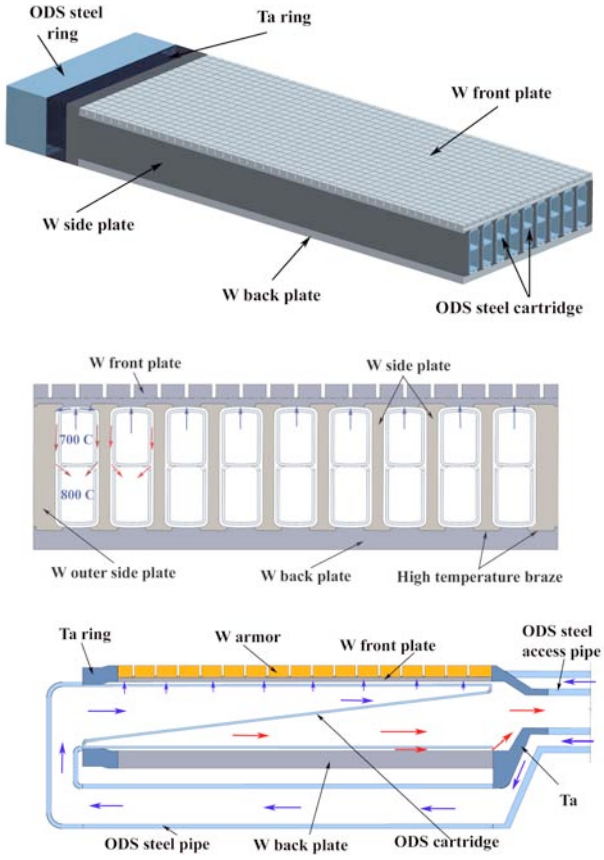

Fig. 4. Drawing of the plate divertor, showing the steel inlet cartridges inserted into the substrate, the castellated armor and the transition joints: a) elevation view, b) cross section, c) flow paths for inlet, outlet and slot jet.

Figure 3 shows clearly that the finger design removes a greater incident heat flux with a lower pumping power

penalty, but it does that with considerably increased complexity. The characteristic scale length of finger divertor elements is of the order of 1.5 cm; approximately ½ million fingers would be needed to cover all divertor targets of a 1000 MW plant. On the other hand, Figure 3 also clearly demonstrates that the plate divertor becomes increasingly challenging when the heat flux exceeds 10 MW/m^2. The integrated plate/finger concept is particularly useful in these cases, since the more complex fingers can be used only in locations where the anticipated heat flux is above 10 MW/m^2. For the current ARIES-ACT1 design, the simpler plate-type divertor with a linear slot jet appears to be an acceptable choice.

Figure 4 shows several drawings of the plate divertor. Coolant enters through a steel manifold into a set of parallel steel cartridges that slide into the W-alloy housing. Coolant is forced through a slot at the plasma-facing surface, after which it impinges on the heated surface and then travels along the side of the cartridge into the outlet manifold. Detailed thermal and inelastic stress analysis has been performed on this design concept, showing that a heat flux of 10 MW/m^2 can be accommodated without exceeding any design limits.[11]

IV. FIRST WALL AND BLANKET

IV.A. Overall Concept

The ARIES-ACT1 breeding blanket is derived from the ARIES-AT blanket concept.[12] It uses a double-shell design in which the coolant passes through an outer annular region before turning 180° at the top of the power core to return through the central duct (see Figure 5). On the first pass, the coolant velocity along the first wall is high in order to allow effective removal of surface heating. The coolant velocity is much lower in the large central duct, where most of the neutron heating is deposited.

Each sector contains three blanket segments – one inboard and two outboard. Each segment consists of parallel ducts containing an inner and outer shell. On the side walls of each segment, a thicker SiC plate is needed to support the coolant pressure. The outer annular region contains grids running vertically along the flow direction. These grids stiffen the module to accommodate internal pressure of the order of 2 MPa, as described below.

Table III summarizes the operating conditions in the breeding blanket. The bulk average outlet temperature is allowed to exceed the structure temperature limit because the annular channel arrangement cools the SiC with inlet coolant. The flow in each of the three blanket segments is tailored to the local surface and volumetric heating in order to maintain the same bulk coolant temperatures. Only worst-case peak values are presented in the table.

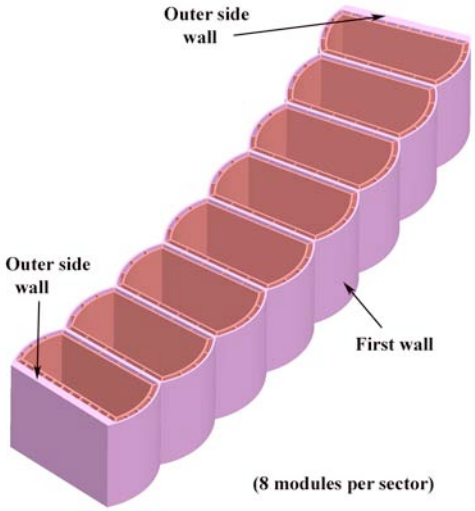

Fig 5. Inboard blanket cross section at midplane

TABLE III. ARIES ACT1 Breeding Blanket Parameters

Parameter	Value	Units
Coolant	PbLi	
Peak first wall heat flux	0.30	MW/m^2
Average first wall heat flux	0.24	MW/m^2
Coolant inlet temperature	740	C
Coolant outlet temperature	1030	C
Peak structure temperature	960	C
Peak first wall coolant velocity	4	m/s
Peak central duct coolant velocity	17	cm/s
Total surface heating	128	MW
Total volumetric heating	1560	MW
Maximum pressure in access pipes	2.8	MPa
Max pressure in outer blanket duct	1.95	MPa
Max pressure across inner duct	0.3	MPa
SiC/SiC stress limit	190	MPa

IV.B. MHD Considerations and Pressure Drop

The exclusive use of electrically insulating SiC structures in contact with PbLi coolant is expected to reduce the MHD pressure drop considerably, making it feasible to design a blanket pressure vessel that can withstand the pressure stresses (as well as thermal stresses). The pressure gradient in a 2-dimensional straight duct with uniform magnetic field is quite low, because that geometry forces induced currents to pass through very thin boundary layers. The high electrical resistance of these thin boundary layers keeps the magnitude of the currents low.

However, any real blanket requires coolant manifolds, bends, expansions and contractions, and routing through varying toroidal and poloidal fields. The resulting 3-dimensional MHD effects can be large, and can dominate the pressure drop, flow distribution and velocity

profiles in the blanket. 3D effects occur when the electric potential is "unbalanced" from ideal 2D profiles, resulting in "short circuits" within the bulk of the coolant, away from the boundary layers.

The voltage across any duct in the direction perpendicular to the magnetic field, is related to the electric field induced by the fluid velocity:

$$V_{ab} = \int_a^b E \bullet dl = \int_a^b u \times B \bullet dl$$

where *a* and *b* are the locations of the two walls. If we can maintain constant voltage along the direction of flow, then we can minimize the generation of 3D currents.

Figures 6a and 6b show several design elements that are expected to have smaller or larger 3D effects. For example, a contraction or expansion of a duct in the direction perpendicular to B does not create a voltage imbalance, because the higher velocity in the smaller flow area is balanced exactly by the smaller integration path. Conversely, a contraction in the same direction as B leads to higher velocity with the same integration path, hence a parallel voltage difference. By avoiding "bad" design elements, we hope to maintain the flow in a quasi-2D condition with only minor perturbations to the fully-developed currents and velocities.

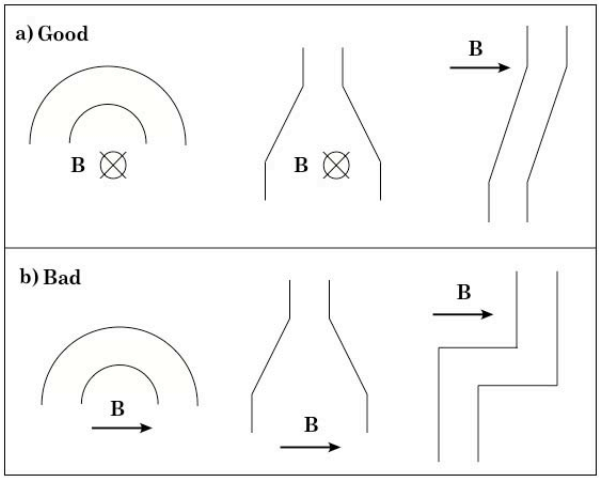

Fig. 6. Design elements that produce (a) small 3D effects or (b) large 3D effects.

A technique for estimating the added 3D pressure drop (above and beyond the normal 2D pressure gradient) from individual elements of a cooling system has been used for many years.[13] Semi-empirical correlations have been collected for various geometries and wall conductance ratios, and placed in a form related to the fluid inertia ($\rho u^2/2$), the MHD interaction parameter (N) and a semi-empirical constant k:

$$\Delta p_{3D} = kN\left(\rho u^2/2\right)$$

For flows with geometrical changes in a uniform magnetic field typically $0.25 < k < 2$. For a change in transverse field strength, k~0.1–0.2 (depending on the abruptness of the change in B). For an inlet or outlet manifold, Smolentsev *et al.* recommended k=1.5.[14]

We performed a thorough examination of the flow paths from the inlet ring headers all the way through the power core and back to the outlet ring headers in order to apply "good" MHD design principles to the maximum extent possible. One location that could not be simplified is the inlet/outlet manifold located at the bottom of the power core. In this region, a single annular access pipe enters the power core and must be subdivided into many parallel channels. We attempted to maintain as much symmetry as possible in the central duct outlet manifold region (see Figure 7) in order to maintain uniform flow distribution between parallel ducts. The pressure drop in this region is probably tolerable. Some recent efforts to analyze this uniquely difficult part of the flow path suggest this concept is feasible,[15,16] but further experimental and modeling studies are needed.

The inlet manifolds for the annular outer channels is an ongoing subject of study within the project. There are many more parallel channels in the outer annulus, and they cannot be simply connected as with the outlet ducts. Some form of physical or MHD orifices (*e.g.,* using the concept of "flow balancing" [17]) may be required; again, R&D is needed to validate this concept.

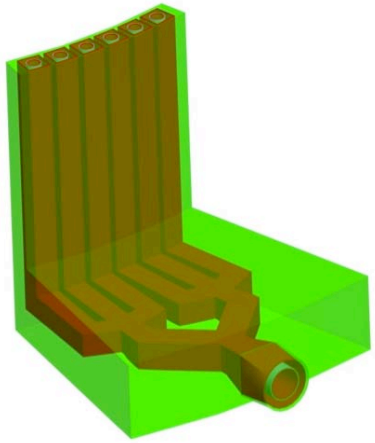
Fig. 7. Inlet manifolding concept for the inner ducts.

In order to evaluate pressure stresses in the blanket and access pipes, pressure drops were estimated using analytic formulas for 2D pressure gradient and the semi-empirical formula above for 3D effects. The static head due to gravity is also major contributor to the local pressures. It is important for safety reasons to locate the PbLi heat exchanger above the highest location in the

blanket to encourage thermal convection under loss-of-flow accidents. Considering these competing needs, we located the heat exchanger just 4 m above the highest point in the blanket. Pressures in the current design are summarized in Table III.

IV.C. Thermal Analysis

The blanket, including all walls and cooling channels, was modeled in 2D in order to obtain the temperature distribution both radially and axially (along the direction of flow). The fluid enters at the bottom in the outer channels and returns through the central duct. We assume the fluid is well mixed at the top bend. Conduction is allowed between the inner and outer ducts; in fact, substantial heat is exchanged in this way. The energy equation is solved in this domain, allowing for volumetric heating and nonuniform velocity profiles:

$$u(x)\frac{\partial e(x,z)}{\partial z} = k\frac{\partial^2 T(x,z)}{\partial x^2} + Q(x)$$

This equation is converted to an initial value problem and solved by relaxing an initial guess of the temperature profile toward a steady state condition in the equation:

$$\frac{\partial e}{\partial t} = k\frac{\partial^2 T}{\partial x^2} + Q - u\frac{\partial e}{\partial z} = 0$$

A special issue arises with heat transfer in the curved first wall ducts. As shown in Figure 8, curvature leads to a variation in path length along magnetic field lines from one side of the duct to the other; this leads to a variation in the effective Hartmann number, which then leads to varying drag on the fluid. Detailed studies suggest that a good approximation of the velocity profile can be made by assuming the velocity is inversely proportional to the path length of the magnetic field, which implies stagnated regions in the corners[18]. We included this feature in the thermal analysis, and found it contributes about 30°C additional temperature rise at the plasma-facing surface. Figure 9 shows the temperature profiles *vs.* distance from the plasma-facing surface at three vertical locations (bottom, middle and top). The radial decay in volume heating is apparent in the central duct. The effectiveness of the annular design in keeping the structures cooler than the peak temperature in the PbLi is also apparent.

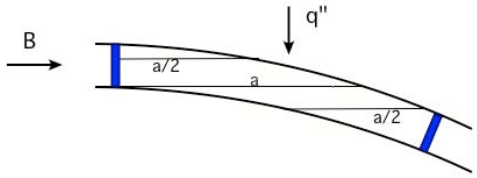

Fig. 8. Geometry of the curved first wall

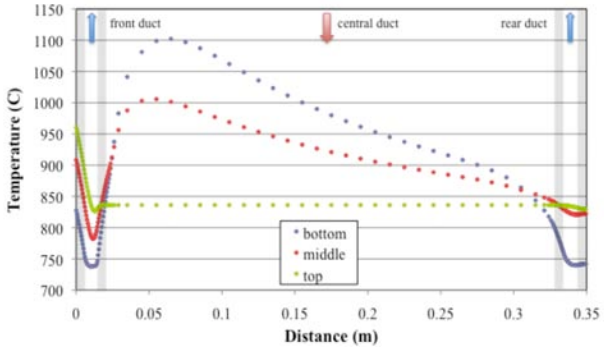

Fig. 9. 2D thermal analysis of the blanket

IV.D. Stress Analysis

Detailed stress analyses were performed on the inboard blanket. Space limitations prevent a comprehensive treatment here. One issue of particular concern is the pressure stress in the modules. The maximum allowable pressure stress restricts the allowable MHD pressure drop, and also determines wall thicknesses, which themselves determine both cost and tritium breeding capability of the power core. Figure 10 illustrates the importance of the grids interconnecting the inner and outer blanket ducts. For this calculation, we assumed a static pressure of 0.8 MPa from the coolant weight near the bottom of the blanket, and varied the pressure difference across the inner duct due to MHD. For SiC/SiC$_f$ composite, our best guidance to date is to maintain the combined primary and secondary stress below 190 MPa[19]. We allocated 100 MPa to primary stress alone, in order to leave margin for thermal stresses. Figure 10 shows a substantial design margin in the case with ribs brazed on both sides.

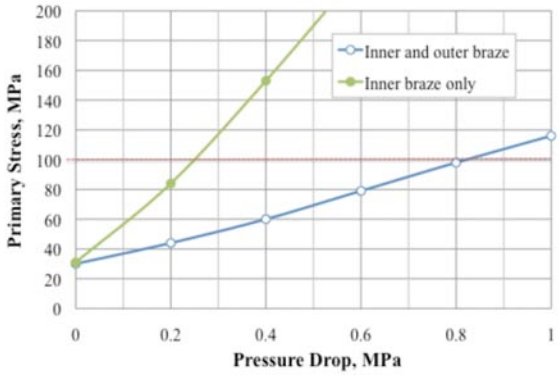

Fig. 10. Pressure stress reduction achieved by brazing the inner and outer blanket pipes

V. POWER CYCLE

High thermal conversion efficiency has been identified in previous ARIES studies as a major factor that enables high performance with only a modest power core size and modest power density. Constraints on other

systems become significantly less challenging when the conversion efficiency is high.

The helium Brayton cycle has been used in previous ARIES designs. It can deliver high conversion efficiency when the turbine inlet temperature is sufficiently high, as it certainly is for the ACT1 advanced blanket concept. Alternatives include a supercritical CO_2 Brayton cycle[20] or a water-based Rankine cycle (either subcritical or supercritical). Water is generally avoided in our designs in order to reduce tritium inventory and tritium handling concerns, and to eliminate any potential for liquid metal/ water reactions causing large safety issues. For the present study, we chose to adopt the He Brayton cycle for which we have greater experience.[21]

As compared with the ARIES-AT power core, which was cooled only by PbLi, we need to extract heat from both He and PbLi in the ACT1 power core and then pass it to a common secondary helium coolant that feeds the main turbine. Heat sources include surface heating, volumetric nuclear heating and heat deposited into the coolants by friction or MHD losses. Heat is passed in series, starting from the He-cooled steel components (the shield and divertor) and then finally the PbLi-cooled blanket.

Figure 11 summarizes the primary and secondary coolant temperatures from the shield, divertor and blanket. The heat exchanger temperature drop from He to He was assumed to be at least 50 C, whereas He to PbLi could be as low as 30 C. Inlet and outlet coolant temperatures must be chosen to account for the total power removed in each component, and constraints from multiple structural materials must be considered. This appears in Figure 11 as a mismatch at the divertor exit.

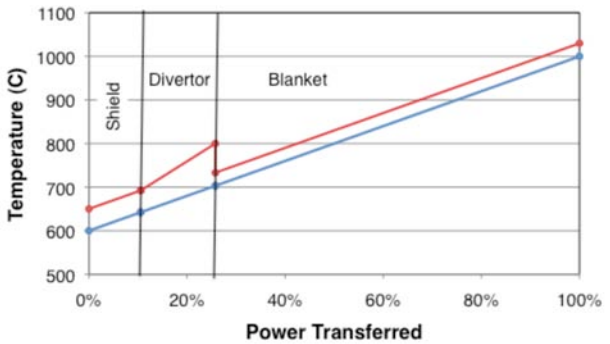

Fig. 11. Thermal power handling in the primary heat exchanger. The top line represents the primary coolant and the bottom line represents the secondary coolant.

The operating point for the power cycle depends on many factors, including the turbine inlet temperature, compression ratio, pressure loss ratio, rejection temperature and component efficiencies.[21] Figure 12 shows how the cycle efficiency and power core inlet temperature depend on compression ratio. The optimum compression ratio results in an inlet temperature too high for the structural ring, so we chose to operate slightly off optimium, where the cycle efficiency is 57.9% and the primary heat exchanger secondary side inlet temperature is 600 C.

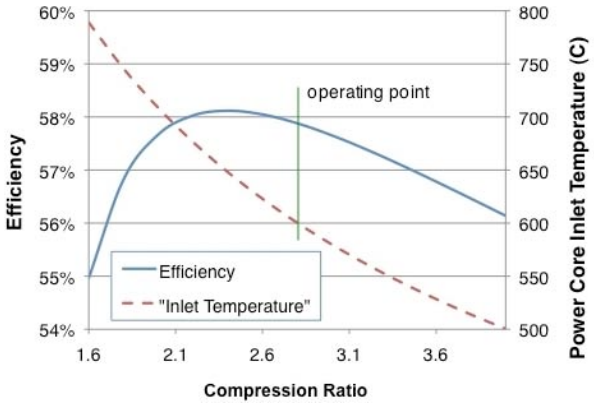

Fig. 12. Operating point for the ARIES-ACT1 power conversion system

VIII. R&D NEEDS

As in any conceptual design of a future fusion power plant, uncertainties exist as a result of the limited existing database and extrapolations that account for anticipated future progress. Many of the engineering challenges relate to fabrication and materials behavior. Table IV summarizes some of the top level R&D needs for the ARIES-ACT1 power plant design. These issues have been identified in previous studies, and already are the subject of ongoing R&D programs.

TABLE IV. R&D needs for ARIES-ACT1

Characterization of the steady and transient surface heat loads on plasma-facing components
MHD effects on flow and heat transfer
Tritium containment and control
Fabrication, assembly and joining of complex structures made of SiC composites, tungsten alloys, and low activation ferritic steels.
Mechanical behavior of steel, W and SiC structures, including fracture mechanics, creep/fatigue, and irradiation effects. Failure modes and rates.
Determination of upper and lower temperature limits of W alloys and advanced ferritic steels.
Fluence lifetime of components under anticipated loading conditions.

ACKNOWLEDGMENTS

Funding for this work was provided by the US Department of Energy under grant DE-FG02-04ER54757.

REFERENCES

1. F. NAJMABADI *et al.*, "Re-examination of visions for tokamak power plants: ARIES-ACT study," *these proceedings*.
2. F. NAJMABADI *et al.,* "The ARIES-AT advanced tokamak, Advanced technology fusion power plant," *Fusion Engineering and Design* **80** (2006) 3–23.
3. X. R. WANG, M. S. TILLACK, S. MALANG, F. NAJMABADI and the ARIES Team, "Overall power core configuration and system integration for the ARIES-ACT1 fusion power plant," *these proceedings*.
4. L. EL-GUEBALY, T. HUHN, A. ROWCLIFFE, S. MALANG and the ARIES-ACT Team "Design challenges and activation concerns for ARIES vacuum vessel," *these proceedings*.
5. M. S. TILLACK, X. R. WANG, J. PULSIFER, I. SVIATOSLAVSKY and the ARIES Team, "ARIES-ST plasma-facing component design and analysis," *Fusion Engineering and Design* **49-50** (2000) 363.
6. M. S. TILLACK, A. R. RAFFRAY, X. R. WANG, S. MALANG, S. ABDEL-KHALIK, M. YODA and D. YOUCHISON, "Recent US activities on advanced He-cooled W-alloy divertor concepts for fusion power plants," *Fusion Engineering and Design* **86** (2011) 71-98.
7. P. NORAJITRA, R. GINIYATULIN, T. IHLI, G. JANESCHITZ, W. KRAUSS, R. KRUESSMANN, V. KUZNETSOV, I. MAZUL, V. WIDAK, I. OVCHINNIKOV, R. RUPPRECHT, "He-cooled divertor development for DEMO," *Fusion Engineering and Design* **82** (2007) 2740.
8. J. RADER, B. MILLS, D. L. SADOWSKI, M. YODA and S. I. ABDEL-KHALIK, "Verification of thermal performance predictions of prototypical multi jet impingement helium-cooled divertor module," *these proceedings.*
9. D. NAVAEI, X. R. WANG, M. S. TILLACK, S. MALANG and the ARIES Team, "Elastic-plastic analysis of transition joints for high performance divertor target plate," *Fusion Science and Technology* **60** (1) July 2011, 233-237.
10. ANSYS Inc., ANSYS 12.0 Documentation, 2009.
11. X. R. WANG, S. MALANG, A. R. RAFFRAY and the ARIES Team, "Design optimization of high performance helium-cooled divertor plate concept," *Fusion Science and Technology* **56** (2009) 1023.
12. A. R. RAFFRAY, L. EL-GUEBALY, S. MALANG, I. SVIATOSLAVSKY, M. S. TILLACK, X. WANG, and the ARIES Team, "Advanced power core system for the ARIES-AT power plant," *Fusion Engineering and Design* **82** (2007) 217–236.
13. O. LIELAUSIS, "Liquid metal magnetohydrodynamics," in *Atomic Energy Review* **13** (3), IAEA Vienna, 1975.
14. S. SMOLENTSEV, C. WONG, S. MALANG, M. DAGHER, M. ABDOU, "MHD considerations for the DCLL inboard blanket and access ducts," *Fusion Engineering and Design* **85** (2010) 1007–1011.
15 N. B. MORLEY, M.-J. NI, R. MUNIPALLI, P. HUANG, M. A. ABDOU, "MHD simulations of liquid metal flow through a toroidally oriented manifold," *Fusion Engineering and Design* **83** (2008) 1335–1339.
16. T. Q. HUA and B. F. PICOLOGLOU, "Magneto-hydrodynamic flow in a manifold and multiple rectangular coolant ducts of self-cooled blankets," Fusion Technology 19 (1991) 102-112.
17. M. S. TILLACK and N. B. MORLEY, "Flow balancing in liquid metal blankets," *Fusion Engineering and Design* **27** (1995) 735-741.
18. L BÜHLER and L. GIANCARLI, "Magnetohydrodynamic flow in the European SCLL blanket concept," Forschungszentrum Karlsruhe report FZKA 6778, 2002.
19. A. R. RAFFRAY, R. JONES, G. AIELLO, M. BILLONE, L. GIANCARLI, H. GOLFIER, A. HASEGAWA, Y. KATOH, A. KOHYAMA, S. NISHIO, B. RICCARDI and M. S. TILLACK, "Design and material issues for SiCf/SiC-based fusion power cores," *Fusion Engineering and Design* **55** (2001) 55-95.
20. P. SARDAIN, D. MAISONNIER, M. MEDRANO, B. BRAÑAS, D. PUENTE, E. ARENAZA, B. HERRAZTI, A. PAULE, A. ORDEN, M DOMÍNGUEZ and R. STAINSBY, "Alternative power conversion cycles for He-cooled fusion reactor concepts," Proceedings of IAEA Technical Meeting "First Generation of Fusion Power Plants: Design and Technology", Vienna, 20-22 June 2007, IAEA-TM-32812, 2009.
21. S. MALANG, H. SCHNAUDER and M. S. TILLACK, "Combination of a self-cooled liquid metal breeder blanket with a gas turbine power conversion system," *Fusion Engineering and Design* **41** (1998) 561.